Disorder-induced effects in high-harmonic generation process in fullerene molecules

H.K. Avetissian, ¹ S. Sukiasyan, ^{1,2} H.H. Matevosyan, ³ and G.F. Mkrtchian ^{1,*}

¹ Centre of Strong Fields Physics at Research Institute of Physics,

Yerevan State University, Yerevan 0025, Armenia

² Max-Planck-Institut für Kernphysik, Saupfercheckweg 1, 69117 Heidelberg, Germany

³ Institute of Radiophysics and Electronics NAS RA, Ashtarak 0203, Armenia

The objective of this article is to investigate the profound nonlinear optical response exhibited by inversion symmetric fullerene molecules under the influence of different types of disorders described by the Anderson model. Our aim is to elucidate the localization effects on the spectra of high harmonic generation in such molecules. We show that the disorder-induced effects are imprinted onto molecules' high-harmonic spectrum. Specifically, we observe a presence of strong even-order harmonic signals already for relatively small disorders. The odd-order harmonics intrinsic for disorder-free systems are generally robust to minor disorders. Both diagonal and off-diagonal disorders lift the degeneracy of states, opening up new channels for interband transitions, leading to the enhancement of the high-harmonic emission. The second harmonic signal has a special behavior depending on the disorder strength. Specifically in the case of diagonal disorder, the second harmonic intensity exhibits a quadratic scaling with the disorder strength, which enables the usage of the harmonic spectrum as a tool in measuring the type and the strength of a disorder.

I. INTRODUCTION

High harmonic generation (HHG) is a nonlinear key process[1] in strong-field physics, which has made great achievements over the past decades in the gaseous phase of matter. Since the discovery of HHG in solids [2–7] and novel nanostructures [8] of fascinating properties, much theoretical (for review see [9] and references therein) and experimental [10-12] attention has been paid to the multiphoton and HHG processes in novel nanostructures. The interest in the HHG process is huge. Particularly, it gives an access to the frequency range that is difficult to achieve in other ways [13], and thanks to the extremely large coherent bandwidth of harmonic spectra HHG enables spectroscopy in attosecond resolution [14]. According to the HHG spectra in crystals, one can observe the dynamical Bloch oscillations [6], Peierls [15], and Mott [16] transitions. The understanding of the high-harmonic spectrum can help in reconstruction of the electronic [17] and topological properties of the materials [18–20]. The generation of harmonics has recently been reported in liquids [21] and in amorphous solids [22], which ensures that the periodicity is not a necessary condition for HHG in condensed matter systems. Some theoretical works found that liquids [23–25], doped materials [26–29], solutions [30], and disordered semiconductors [31–33] can produce harmonics efficiently.

The disorder is always present in crystals, and it is of particular interest to investigate its influence on the HHG process in novel nanostructures. Since the fundamental works by Anderson [34] and co-workers [35], it is known that the presence of the disorder in a lattice structure is a key factor defining the extension of the electronic wave function. Depending on the dimensionality of the system

* Email: mkrtchian@ysu.am

Anderson localization changes its character [36]. Particularly, even for small disorder strengths, all states in a disordered system with dimension below 2 are localized in a small fraction of the lattice. It is well known that the HHG process is very sensitive to electronic wave function extension [37] and therefore high harmonic spectroscopy can reveal disorder-induced Anderson localization. Latter has been shown for finite linear chain [38]. Anderson localization is a fundamental wave phenomenon and takes place also for finite nanostructured materials with a sufficiently large number of sites. For systems with a finite number of atoms, particular interest represent the planar quantum dots based on graphene or the case of fullerenes with lattice topologies of nodes distributed over a closed surface. The most known fullerene is C_{60} [39], the discovery of which triggered the study of many other carbon nanostructures [8, 40]. Today, graphene quantum dots [41] and fullerene molecules [42] are promising materials for extreme nonlinear optics. Theoretically strong HHG emission is predicted in C_{60} and C_{70} molecules [43–46]. The analysis in mentioned works is for disorder-free systems and it is unclear how the disorder leaves its mark on the HHG and sub-cycle electronic response. In recent years the effect of the disorder, impurities and vacancies on HHG in solid materials has been studied in the papers [28–31, 33, 47–50]. These investigations reveal situations where an imperfect lattice might actually amplify HHG in comparison to a perfectly ordered lattice [28, 29, 47, 49]. In finite systems, like fullerene molecules, our current understanding indicates that the effect of the disorder on the electromagnetic response is predominantly confined to the linear regime of interaction [51].

In the present work, we develop a microscopic theory for the nonlinear interaction of the fullerene molecules with the strong electromagnetic radiation of linear polarization taking into account diagonal and off-diagonal disorders. We also consider the electron-electron interaction (EEI) in the Hartree-Fock approximation [46]. In particular, we consider C_{60} and C_{180} molecules with the same icosahedron point group symmetry, but with different number of atoms, which allows one to study the size effect as well. By means of the dynamical Hartree-Fock approximation, we study the dependence of the HHG spectrum on the disorder type and strength. Our concept can be easily generalized to other molecules of this family.

This paper is organized as follows. In Sec. II, the model and the basic equations are formulated. In Sec. III, we represent the main results. Finally, conclusions are given in Sec. IV.

II. THE MODEL AND THEORETICAL METHODS

Our target represents a carbon based nanostructure, with sites distributed over a closed surface, interacting with mid-infrared laser pulse. In particular, we consider the lattice topology of fullerene buckyballs C_{60} and C_{180} . Both molecules are invariant under the inversion with respect to the center of mass and have icosahedral point group (I_h) symmetry. We assume neutral fullerene molecules, described within the tight-binding theory where the interball hopping is much smaller than the on-ball hopping, and the EEI is described within the extended Hubbard approximation [52]. The total Hamiltonian reads:

$$\widehat{H} = \widehat{H}_{TB} + \widehat{H}_{C} + \widehat{H}_{int}, \tag{1}$$

where

$$\hat{H}_{TB} = \sum_{i\sigma} \epsilon_i c_{i\sigma}^{\dagger} c_{j\sigma} - \sum_{\langle i,j \rangle \sigma} (t_{ij} + \beta_{ij}) c_{i\sigma}^{\dagger} c_{j\sigma} \qquad (2)$$

is the free, tight-binding, fullerene Hamiltonian. Here $c_{i\sigma}^{\dagger}$ $(c_{i\sigma})$ creates (annihilates) an electron with the spin polarization $\sigma = \{\uparrow, \downarrow\}$ at the site i ($\overline{\sigma}$ is the opposite to σ spin polarization), ϵ_i is the energy level at the site i, and $\langle i,j \rangle$ runs over all the first nearest-neighbor hopping sites with the hopping integral $(t_{ij} + \beta_{ij})$ between the sites i and j. In the absence of disorder, $\epsilon_i = 0$, $\beta_{ij} = 0$, and the hopping integral between the nearestneighbor atoms at positions \mathbf{r}_i and \mathbf{r}_j is approximated by $t_{ij} = t_0 + \alpha (d_0 - |\mathbf{r}_i - \mathbf{r}_j|)$ [43]. Taking $d_0 = 1.54\text{Å}$ and by fitting the energy gap for C_{60} , we have determined the average hopping constant $t_0 = 2.17$ eV and the electron-lattice coupling constant $\alpha = 3.52 \text{ eV/Å}$. Input coordinates for the C_{60} and C_{180} are generated with the program Fullerene via a face-spiral algorithm [42]. The initial structure is further optimized by a force field specifically designed for fullerenes [53]. In the real-space tight-binding Hamiltonian (2) the disorder is introduced with randomly distributed site energies ϵ_i , called as diagonal disorder, or with random hopping integrals β_{ij}

called as off-diagonal disorder. We assume for the random variables ϵ_i and β_{ij} to have probability distributions $P(\epsilon_i, V_{\text{on}})$ and $P(\beta_{ij}, V_{\text{off}})$, where

$$P(x,\Delta) = \begin{cases} \frac{1}{2\Delta}, & -\Delta \le x \le \Delta \\ 0, & \text{otherwise} \end{cases}$$
 (3)

Here the quantities $V_{\rm on}$ and $V_{\rm off}$ are the distribution widths describing the strength of the disorders. Similar to other macroscopic or mesoscopic systems, fullerene molecules are subject to different types of disorders [54]. Diagonal disorder arises from impurities or the randomness of the surrounding medium [55, 56], while off-diagonal disorder emerges from fluctuations in bond lengths around their average value caused by lattice distortions [51]. The assessment of disorder strength for both types of disorders suggests that a value $V_{\rm on,off} \sim 0.1t_0$ would be a reasonable estimate.

The second term in the total Hamiltonian (1) describes the extended Hubbard Hamiltonian with the U and Vterms included. Within the Hartree-Fock approximation, the Hamiltonian $\hat{H}_{\rm C}$ is approximated by

$$\widehat{H}_{C}^{HF} = U \sum_{i} (\overline{n}_{i\uparrow} - \overline{n}_{0i\uparrow}) n_{i\downarrow}
+ U \sum_{i} (\overline{n}_{i\downarrow} - \overline{n}_{0i\downarrow}) n_{i\uparrow} + \sum_{\langle i,j \rangle} V_{ij} (\overline{n}_{j} - \overline{n}_{0j}) n_{i}
- \sum_{\langle i,j \rangle \sigma} V_{ij} c_{i\sigma}^{\dagger} c_{j\sigma} \left(\rho_{ji}^{(\sigma)} - \left\langle c_{i\sigma}^{\dagger} c_{j\sigma} \right\rangle_{0} \right),$$
(4)

with on- and inter-site Coulomb repulsion energies U and V_{ij} , respectively, where $n_{i\sigma}=c_{i\sigma}^{\dagger}c_{i\sigma}$ is the density operator and $n_i=n_{i\uparrow}+n_{i\downarrow}$ is the total electron density for the site i. Here $\overline{n}_{i\sigma}=\left\langle c_{i\sigma}^{\dagger}c_{i\sigma}\right\rangle$ and $\rho_{ji}^{(\sigma)}=\left\langle c_{i\sigma}^{\dagger}c_{j\sigma}\right\rangle$. Since the distance d_{ij} between the nearest-neighbor pairs varies over the system, we scale inter-site Coulomb repulsion as: $V_{ij}=Vd_{\min}/d_{ij}$, where d_{\min} is the minimal nearest-neighbor distance. For all calculations we use the ratio V=0.4U [57]. In this representation the initial density matrix $\rho_{0ji}^{(\sigma)}=\left\langle c_{i\sigma}^{\dagger}c_{j\sigma}\right\rangle_0$ is calculated with respect to the tight-binding Hamiltonian $\widehat{H}_{\mathrm{TB}}$, neglecting the EEI Hamiltonian, i.e. $\widehat{H}_{C}^{HF}=0$.

The last term in the total Hamiltonian (1) is the lightmatter interaction part that is described in the lengthgauge:

$$\hat{H}_{\text{int}} = e \sum_{i\sigma} \mathbf{r}_i \cdot \mathbf{E}(t) c_{i\sigma}^{\dagger} c_{i\sigma}, \qquad (5)$$

where \mathbf{r}_i is the position vector and $\mathbf{E}(t) = f(t) E_0 \hat{\mathbf{e}} \cos \omega t$ represents the electric field, with the frequency ω , amplitude E_0 , polarization vector $\hat{\mathbf{e}}$ and pulse envelope $f(t) = \sin^2(\pi t/\mathcal{T})$, where \mathcal{T} is the pulse duration. From the Heisenberg equation we obtain evolutionary equations for the single-particle density matrix

$$\rho_{ij}^{(\sigma)} = \left\langle c_{j\sigma}^{\dagger} c_{i\sigma} \right\rangle :$$

$$i\hbar \frac{\partial \rho_{ij}^{(\sigma)}}{\partial t} = \sum_{k} \left(\tau_{kj\sigma} \rho_{ik}^{(\sigma)} - \tau_{ik\sigma} \rho_{kj}^{(\sigma)} \right) + (V_{i\sigma} - V_{j\sigma}) \rho_{ij}^{(\sigma)}$$

$$+ e \mathbf{E} \left(t \right) (\mathbf{r}_{i} - \mathbf{r}_{j}) \rho_{ij}^{(\sigma)} - i\hbar \gamma \left(\rho_{ij}^{(\sigma)} - \rho_{0ij}^{(\sigma)} \right),$$

where

$$V_{i\sigma} = \sum_{j\alpha} V_{ij} \left(\rho_{jj}^{(\alpha)} - \rho_{0jj}^{(\alpha)} \right) + U \left(\rho_{ii}^{(\overline{\sigma})} - \rho_{0ii}^{(\overline{\sigma})} \right) \tag{7}$$

and

$$\tau_{ij\sigma} = -\epsilon_i \delta_{ij} + t_{ij} + \beta_{ij} + V_{ij} \left(\rho_{ji}^{(\sigma)} - \rho_{0ji}^{(\sigma)} \right)$$
 (8)

are defined via the density matrix $\rho_{ij}^{(\sigma)}$ and its initial value. In addition, we assume that the system relaxes at a rate γ to the equilibrium $\rho_{0ij}^{(\sigma)}$ distribution. While the evolutionary equations (6) for the single-particle density matrix in the HF approximation offer a reasonably accurate approximation for describing light absorption effects in fullerene molecules even for larger Coulomb interaction energies $U \sim 2t_0 - 4t_0$ [51], it is important to mention that systems with the large U require a treatment beyond the HF approximation [58], such as the Kadanoff-Baym-Keldysh approach [59, 60], to properly account for Coulomb interactions.

The incorporation of disorders into the evolutionary equations, as demonstrated by Eqs. (6), (7), and (8), occurs through dual mechanisms. Firstly, by means of the initial single-particle density matrix $\rho_{0ij}^{(\sigma)}$, which is calculated in relation to the tight-binding Hamiltonian (2). Secondly, through the adjustment of the mean-field hopping integrals (8). In the subsequent analysis, we will explore scenarios in which only one type of disorder is present. In the context of diagonal disorder, we establish β_{ij} as zero, indicating the modification of solely on-site energies. In the case of off-diagonal disorder, ϵ_i is set to zero, signifying the alteration of exclusively hopping integrals. For all results we repeat the calculations with equally distributed variables ϵ_i or β_{ij} according to distribution (3) and then take the ensemble average.

III. RESULTS

A. Eigenstates localization, transition channels and eigenenergies

First we consider the influence of the disorder on the eigenstates and eigenenergies of considered systems prior the interaction with the strong laser pulse. These results are obtained by numerical diagonalization of the tight-binding Hamiltonian (2) including the diagonal and off-diagonal disorders. Numerically diagonalizing the tight-binding Hamiltonian $\hat{H}_{\rm TB}$ we find the eigenstates $\psi_{\mu}\left(i\right)$,

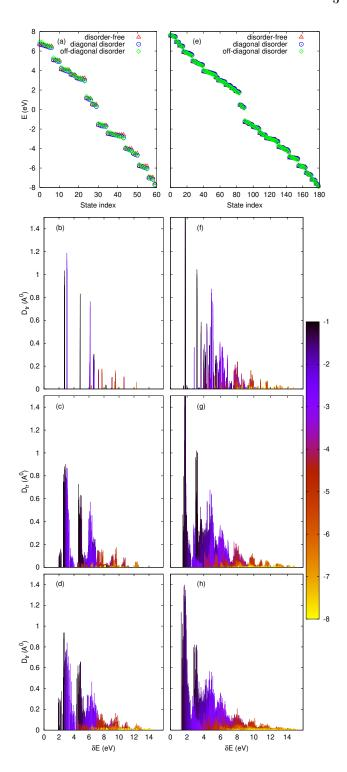


FIG. 1. Eigenenergies of disorder-free and disordered fullerene molecules are displayed for C_{60} (a) and C_{180} (e). The absolute values of matrix elements of the transition dipole moment for interband transitions are shown for C_{60} (b, c, d) and for C_{180} (f, g, h). Panels (b) and (f) correspond to the case without disorders ($V_{\rm on} = V_{\rm off} = 0$). Panels (c) and (g) represent the scenario with only diagonal disorder ($V_{\rm on} = 0.5$ eV, $V_{\rm off} = 0$). Panels (d) and (h) concern the case of solely off-diagonal disorder ($V_{\rm on} = 0$, $V_{\rm off} = 0.5$ eV). The color bar within the figure provides the energy range (in eV) of the valence band.

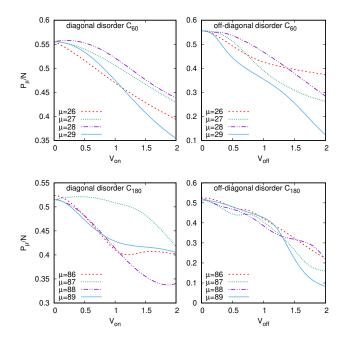


FIG. 2. The normalized inverse participation number for four states near the Fermi level as a function of disorder strength for C_{60} and C_{180} .

eigenenergies ε_{μ} ($\mu=0,1..N-1$), and dipole transition matrix elements $\mathbf{d}_{\mu'\mu}=e\sum_{i}\psi_{\mu'}^{*}(i)\,\mathbf{r}_{i}\psi_{\mu}(i)$. The results are shown in Fig. 1 for C_{60} and C_{180} . Figures 1 (a) and (e) show the eigenspectrum of fullerene molecules without and with disorders included. The differences in the eigenspectrum for the three (off, diagonal and off-diagonal) disorder cases are almost indistinguishable. Compared with the C_{60} molecule, the C_{180} has more degenerated states. In Figs. 1 (b-d,f-h) the absolute value of transition dipole moment versus energy difference is displayed, which shows that both, the diagonal and off-diagonal, disorders lift the degeneracy of states and break the inversion symmetry opening up new channels for interband transitions. Besides, we observe that the first dipole-allowed transition gaps are narrowed. As we will see, these two factors have considerable influences on the HHG spectrum.

In contrast to the eigenspectrum, the eigenstates of the system become partially localized due to the Anderson mechanism. To provide a quantitative characterization of localization in the μ -th eigenstates, we also calculate the inverse participation number

$$P_{\mu} = \left(\sum_{i=0}^{N-1} |\psi_{\mu}(i)|^{4}\right)^{-1}, \tag{9}$$

which provides a measure of the fraction of sites over which the wavepacket is spread [61]. In the case of delocalized states evenly distributed over the entire system, the inverse participation ratio becomes equal to N, while for a state located in a single site, $P_{\mu} = 1$. For the finite systems under consideration, where the thermodynamic limit is not applicable, the inverse participation number serves as an indicator of the localization tendency. Additionally, we will explore disorders with strengths comparable to or smaller than the nearest neighbor hopping matrix element, t_0 . Although the localization arises from the Anderson mechanism, it should be noted that for moderate disorder strengths, we will have partial localization. To achieve complete localization, disorders with strengths significantly larger than the hopping matrix element would be required, which is not experimentally feasible for the considered systems. As illustrated in Fig. 2, we plot the normalized inverse participation number P_{μ}/N for four states near the Fermi level as a function of disorder strength for C_{60} and C_{180} molecules. From Fig. 2, it becomes evident that there is a clear trend towards localization in both cases. The localization effect is weak and more pronounced in the case of off-diagonal disorder. We further investigate the impact of localized eigenstates on the charge distribution within the fully-filled valence band. To visualize this, we construct the initial density matrix $\rho_{0ij}^{(\sigma)}$ by populating electron states in the valence band according to the zero temperature Fermi-Dirac distribution $\rho_{0ij}^{(\sigma)} = \sum_{\mu=N/2}^{N-1} \psi_{\mu}^{*}(j) \psi_{\mu}(i)$. Fig. 3 displays the equilibrium site occupations, $n_i = \rho_{0ii}^{(\uparrow)} + \rho_{0ii}^{(\downarrow)}$, for C₆₀ (upper panel) and C₁₈₀ (lower panel) respectively. We observe a significant change in the initial configuration when diagonal disorder is introduced, deviating from the initially homogeneous distribution. However, in the presence of off-diagonal disorder, despite the localization of individual states, the initial configuration remains relatively close to a homogeneous distribution.

B. Disorder-induced effects in HHG process

To study the HHG process in C_{60} and C_{180} fullerene molecules we evaluate the high-harmonic spectrum by Fourier Transformation of the dipole acceleration, $\mathbf{a}(t) = d^2\mathbf{d}(\mathbf{t})/dt^2$, where the dipole momentum is defined as $\mathbf{d}(t) = e \sum_{i\sigma} \mathbf{r}_i \rho_{ii}^{(\sigma)}(t)$:

$$\mathbf{a}\left(\Omega\right) = \int_{0}^{\mathcal{T}} \mathbf{a}\left(t\right) e^{i\Omega t} W\left(t\right) dt, \tag{10}$$

where W(t) is the window function to suppress small fluctuations [62] and to decrease the overall background (noise level) of the harmonic signal. As a window function we take the pulse envelope f(t). We assume the excitation frequency $\omega=0.2~{\rm eV}/\hbar$ is much smaller than the typical gap $\sim 2~{\rm eV}$.

The linearly polarized laser pulse is assumed to have 20 wave cycles: $T = 40\pi/\omega$. To obtain the mean picture which does not depend on the orientation of the molecule with respect to laser polarization, we take the wave polarization vector as $\hat{\mathbf{e}} = \{1, 1, 1\}$. The Coulomb repulsion energy due to the screening can be considered to be in the

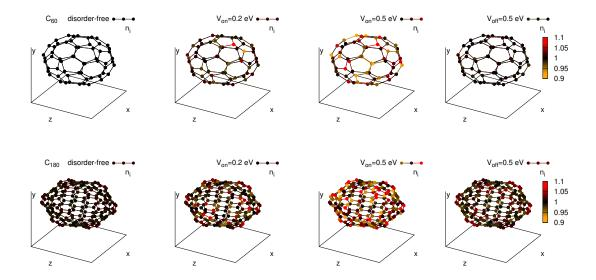


FIG. 3. The equilibrium occupations n_i of sites in the 3D color-mapped molecular structures for C_{60} (upper panel) and for C_{180} (lower panel). The first configuration is disorder free. Next 3 configurations are for diagonal disorder, $V_{\rm on}=0.2$ and 0.5 eV, and for off-diagonal disorder $V_{\rm off}=0.5$ eV.

range 1-3.0 eV [57, 63]. The spectra are calculated for moderate Coulomb repulsion energy, U=2 eV. While reported relaxation rates for fullerene molecules typically are around $0.01t_0$ [51] for linear optical effects, we adopt a value of $\hbar\gamma=0.1$ eV in this study. This choice is motivated by the presence of disorder and high-intensity laser excitation, which are expected to enhance the relaxation rate. It is worth noting that the effects investigated in this paper exhibit only a minor dependence on the relaxation rate. For the convenience, we normalize the dipole acceleration by the factor $a_0=e\overline{\omega}^2\overline{d}$, where $\overline{\omega}=1$ eV/ \hbar and $\overline{d}=1$ Å. The power radiated at the given frequency is proportional to $|\mathbf{a}(\Omega)|^2$. The time propagation of Eq. (6) is performed by the eight-order Runge-Kutta algorithm. The time step is taken to be $\Delta t=2\times 10^{-2}$ fs.

Fig. 4 shows the high-harmonic spectra for C_{60} and C_{180} systems in strong laser field. In considered systems for the disorder-free case the inversion symmetry leads to the presence of only odd harmonics in the HHG spectrum. As we mention from Fig. 4, even for small disorder strengths we observe even harmonic signals comparable to odd ones. Due to the size effects even harmonics are more pronounced in C_{60} molecule. The appearance of even-order harmonics is connected with the localization of eigenstates which breaks the inversion symmetry. The odd harmonics, as can be seen in the inset of Fig. 4(b), demonstrate relative stable behavior in the presence of the disorder, especially for the off-diagonal one.

Next we study the dependence of high-harmonic emission on the disorder strength. In Figs. 5 and 6 the HHG spectra up to the 20th harmonics for C_{60} and C_{180} are shown for a range of the diagonal and off-diagonal disorders 0.1-1.0 eV. First we consider the disorder effect

on odd harmonics, which solely represent the HHG spectrum in the disorder-free case. Here we observe a relative stable behavior of C_{180} system changing the disorder strength. The harmonic yield increases slightly with the increase of the diagonal disorder, $V_{\rm on}$, while the effect of the off-diagonal one, $V_{\rm off}$, is not strongly monotonic increasing. The influence of the disorder on the C_{60} system is much more pronounced. Overall we obtain an increase in odd-order high-harmonics emission with increasing the disorder. Particularly, the enhancement caused by the off-diagonal counterpart is by an order higher compared to the diagonal one. Even-order harmonics, which appear due to the breakdown of the symmetry caused by the disorder, increase with the disorder strength. Figs. 5 and 6 show that the effect of the disorder on the evenorder harmonics is much more pronounced in the case of C_{60} system compared to the C_{180} one. The reason for the enhancement of HHG emission lies on the fact that both, the diagonal and off-diagonal disorders lift the degeneracy of states, and the parity of states becomes uncertain opening up new numerous channels for interband transitions. Surprisingly the disorder, being random in nature, does not initiate chaotic behavior in the HHG spectra even for rather large disorder strengths.

Examining Figs. 5 and 6, it becomes evident that the bandwidths of harmonics remain almost resilient to varying disorder strengths. This phenomenon can be attributed to the fundamental underpinnings of HHG within the strong-field regime. In scenarios where perturbation theory is no longer applicable due to the strength of the fields, the generation of high harmonics is governed by sub-cycle nonlinear quantum dynamics, intricately linked to the structure of the pump wave pulse. As the harmonic order increases, harmonics emission primarily

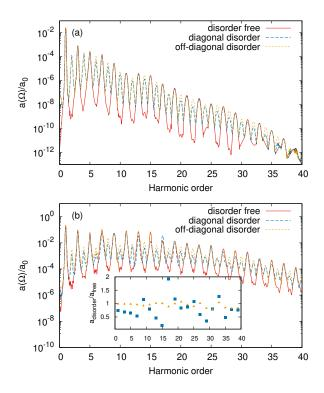


FIG. 4. Normalized HHG spectra, $a\left(\Omega\right)/a_{0}$, in logarithmic scale for C_{60} (a) and for C_{180} (b). For disorders we have taken $V_{\rm on}=0.1~{\rm eV}$ and $V_{\rm off}=0.1~{\rm eV}$. The wave amplitude is taken to be $E_{0}=0.2~{\rm V/\mathring{A}}$. The inset shows the ratio of the spectra with and without disorders for odd harmonics.

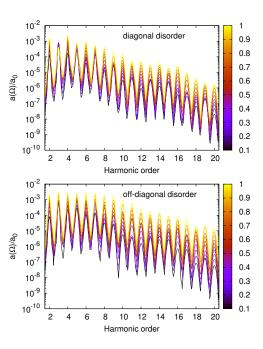


FIG. 5. Normalized HHG spectra for C_{60} in logarithmic scale for a range of the diagonal disorder (upper panel) and off-diagonal disorder (lower panel). The color bar shows the strength of the disorder in eV. Laser parameters same as those in Fig. 4

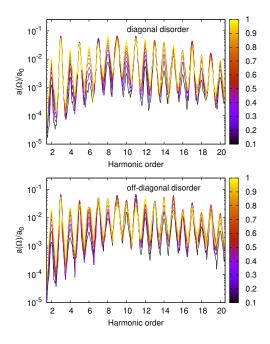


FIG. 6. The same as in Fig. 5, but for C_{180} .

occur in proximity to the peak of the pump wave, ultimately leading to the determination of harmonic bandwidths by pulse duration and wave frequency. It is noteworthy that higher relaxation rates can, in fact, result in a clearer HHG spectrum [64].

Regarding the influence of disorder, as evident from Fig. 1, the presence of disorder opens up novel channels for interband transitions, thereby enhancing the likelihood of multiphoton electron excitation from the valence to conduction bands. This process involves the creation of electron-hole pairs followed by their subsequent recombination, resulting in the emission of high-energy photons. To gain a quantitative understanding of this phenomenon, we employ a Morlet transform of the dipole acceleration

$$\mathbf{a}(t,\Omega) = \sqrt{\frac{\Omega}{\sigma}} \int_{0}^{\tau} d\mathbf{t}' \mathbf{a}(t) \, e^{i\Omega(t'-t)} e^{-\frac{\Omega^{2}}{2\sigma^{2}}(t'-t)^{2}}. \tag{11}$$

For a concrete illustration, we consider the time profiles of the 3rd and 19th harmonics computed through Eq. (11), as depicted in Fig. 7. Irrespective of the presence of disorder, the qualitative behavior remains consistent. For the 3rd harmonic (0.6 eV), which lies below the band gap and is a product of intraband transitions, the time profile exhibits a relatively smooth evolution over time, closely resembling the envelope of the pump wave. Conversely, the 19th harmonic (3.8 eV), arising from interband transitions, reveals a time profile characterized by two distinct bursts within each optical cycle, corresponding to the maxima or minima of the pump wave. Remarkably, these bursts occur in close proximity to the peak of the pump wave.

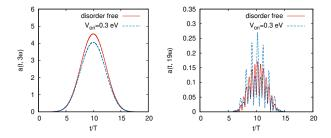


FIG. 7. The time profiles of the 3rd (left panel) and 19th (right panel) harmonics for C_{180} . The interaction parameters are the same as those in Fig. 5. The Morlet transform parameter in Eq. (11) is taken to be $\sigma=15$

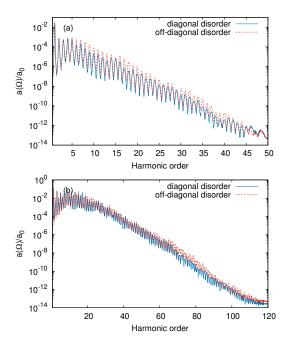


FIG. 8. Comparison of the influence of diagonal $V_{\rm on}=0.5~{\rm eV}$ and off-diagonal $V_{\rm off}=0.5~{\rm eV}$ disorders on the HHG spectra for C_{60} (a) and for C_{180} (b). The wave amplitude is taken to be $E_0=0.2~{\rm V/\mathring{A}}$.

Fig. 8 compares the influences of diagonal and off-diagonal disorders on the HHG spectra for a moderate disorder strength. From this figure we observe, once more, stronger effect of the off-diagonal disorder compared to the diagonal one in the amplification of the HHG yield. The off-diagonal disorder acting on the hopping integral makes electrons more mobile. Besides, the first dipole-allowed transition gaps are narrower for the off-diagonal disorder, cf. Fig 1. As a result, the excitation of electrons from the valence to the conduction band and further intraband excitations to higher levels are more probable for the off-diagonal disorder. In Fig. 9 the residual population of conduction band energy levels is displayed, which confirms the above-mentioned arguments.

In Ref. [46] the suppression of HHG with the increase

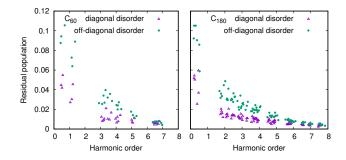


FIG. 9. The residual population of conduction band energy levels for the setup of Fig. 8 for C_{60} (a) and for C_{180} (b).

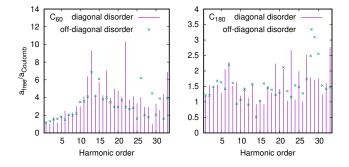


FIG. 10. Coulomb interaction effect on HHG via the ratio of the high-harmonic intensities calculated without and with the Coulomb interaction for C_{60} (a) and for C_{180} (b). For disorders strengths we have taken $V_{\rm on}=0.5$ eV and $V_{\rm off}=0.5$ eV. The wave amplitude is taken to be $E_0=0.2$ V/Å.

of EEI has been found. Latter is connected with the fact that at strong on-site and inter-site electron-electron repulsion the polarizability of molecules, or in other words, electrons migration from the equilibrium states, is suppressed. It is interesting to investigate the interplay of Coulomb and disorder effects. In Fig. 10, the ratio of harmonic intensities without and with the Coulomb interaction is shown. As we observe, in the case of the off-diagonal disorder the Coulomb-induced suppression of HHG is smaller than in the case of the diagonal one. This is connected with the fact that for the off-diagonal disorder the initial configuration is almost homogeneous and close to the disorder-free case, cf. Fig 3.

Finally we turn to the second harmonic signal which is unique for diagnostic tools. In Fig. 11, the nonlinear response of the fullerene molecules, C_{60} and C_{180} , via the scaled second harmonic intensity depending on the diagonal disorder is displayed for different pump wave intensities. As we see, the dependence of second harmonic intensity, I_2 , on the diagonal disorder strength, $V_{\rm on}$, is perfectly described by the law $I_2 \sim V_{\rm on}^2$ for both, C_{60} and C_{180} , systems. For the dependence of second harmonic intensity on the off-diagonal disorder we have not observed such a universal law. Here we report a faster increase of the intensity of the second harmonic with respect to the increase of off-diagonal disorder

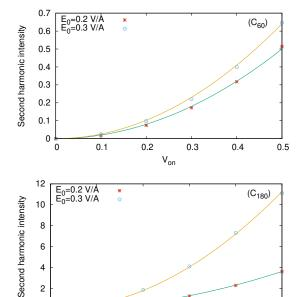


FIG. 11. The nonlinear response of C_{60} and C_{180} via the scaled second harmonic intensity versus the strength of diagonal disorder. By solid lines the fit of the second harmonic intensity by the law: $I_2 \sim V_{0n}^2$ is shown.

V_{on}

0.2

0.3

0.4

0.5

0

0.1

strength, compared to the diagonal one. In particular, at $E_0 = 0.2 \text{ V/Å}$ we have $I_2 \sim V_{\text{off}}^3$ and $I_2 \sim V_{\text{off}}^{5/2}$ dependencies, for C_{60} and C_{180} molecules, respectively. Summarizing, our findings show that the non-linear optical response, in particular the second harmonic signal, can be used as a spectroscopic tool to measure the type and

the strength of the disorder.

IV. CONCLUSION

We have investigated the extreme nonlinear optical response of the carbon-based quantum dots for the case of lattice topologies where sites are distributed over a closed surface, subjected to different types of disorders. In particular, we considered fullerene molecules C_{60} and C_{180} as typical examples of inversion symmetric stable configurations. Solving the evolutionary equations for the singleparticle density matrix, taking into account the manybody Coulomb interaction in the Hartree-Fock approximation, we demonstrate that the disorder-induced effects have strong influence on the emission of high-harmonics. Both diagonal and off-diagonal disorders lift the degeneracy of the states, opening up new channels for interband transitions, leading to the amplification of high-harmonic signals. For the characteristic odd harmonics the effect of disorder is dependent on the type and the strength of the disorder, and on the molecular system. We observe a drastic increase in the intensity of even-order harmonics, making them comparable with the odd ones. The obtained results show that the disorders have their unique footprints in the second harmonic signal, which demonstrates a monotonic increase in intensity with the different power laws for diagonal and off-diagonal disorders, which may allow us to distinguish and measure the disorders type and strengths, paving the way for an optical characterization of the disorder in nanostructures.

ACKNOWLEDGMENTS

The work was supported by the Science Committee of Republic of Armenia, project No. 20TTWS-1C010.

^[1] P. B. Corkum, Plasma perspective on strong field multiphoton ionization, Phys Rev Lett **71**, 1994 (1993).

^[2] S. Ghimire, A. D. DiChiara, E. Sistrunk, P. Agostini, L. F. DiMauro, and D. A. Reis, Observation of high-order harmonic generation in a bulk crystal, Nat Phys 7, 138 (2011).

^[3] B. Zaks, R.-B. Liu, and M. S. Sherwin, Experimental observation of electron-hole recollisions, Nature 483, 580 (2012).

^[4] O. Schubert, M. Hohenleutner, F. Langer, B. Urbanek, C. Lange, U. Huttner, D. Golde, T. Meier, M. Kira, S. W. Koch, et al., Sub-cycle control of terahertz high-harmonic generation by dynamical Bloch oscillations, Nat Photonics 8, 119 (2014).

^[5] G. Vampa, T. J. Hammond, N. Thiré, B. E. Schmidt, F. Légaré, C. R. McDonald, T. Brabec, and P. B. Corkum, Linking high harmonics from gases and solids, Nature 522, 462 (2015).

^[6] T. T. Luu, M. Garg, S. Y. Kruchinin, A. Moulet, M. T. Hassan, and E. Goulielmakis, Extreme ultraviolet highharmonic spectroscopy of solids, Nature 521, 498 (2015).

^[7] S. Ghimire and D. A. Reis, High-harmonic generation from solids, Nat Phys 15, 10 (2019).

^[8] A. K. Geim and I. V. Grigorieva, Van der Waals heterostructures, Nature 499, 419 (2013).

^[9] H. K. Avetissian, G. F. Mkrtchian, and A. Knorr, Efficient high-harmonic generation in graphene with two-color laser field at orthogonal polarization, Phys Rev B 105, 195405 (2022).

^[10] N. Yoshikawa, T. Tamaya, and K. Tanaka, Highharmonic generation in graphene enhanced by elliptically polarized light excitation, Science 356, 736 (2017).

^[11] H. A. Hafez, S. Kovalev, J.-C. Deinert, Z. Mics, B. Green, N. Awari, M. Chen, S. Germanskiy, U. Lehnert, J. Teichert, et al., Extremely efficient terahertz high-harmonic generation in graphene by hot Dirac fermions, Nature 561, 507 (2018).

- [12] G. Le Breton, A. Rubio, and N. Tancogne-Dejean, High-harmonic generation from few-layer hexagonal boron nitride: Evolution from monolayer to bulk response, Phys Rev B 98, 165308 (2018).
- [13] H. K. Avetissian, Relativistic Nonlinear Electrodynamics: The QED Vacuum and Matter in Super-Strong Radiation Fields, Vol. 88 (Springer, 2015).
- [14] F. Krausz and M. Ivanov, Attosecond physics, Rev Mod Phys 81, 163 (2009).
- [15] D. Bauer and K. K. Hansen, High-harmonic generation in solids with and without topological edge states, Phys Rev Lett 120, 177401 (2018).
- [16] R. E. F. Silva, I. V. Blinov, A. N. Rubtsov, O. Smirnova, and M. Ivanov, High-harmonic spectroscopy of ultrafast many-body dynamics in strongly correlated systems, Nat Photonics 12, 266 (2018).
- [17] G. Vampa, T. J. Hammond, N. Thiré, B. E. Schmidt, F. Légaré, C. R. McDonald, T. Brabec, D. D. Klug, and P. B. Corkum, All-optical reconstruction of crystal band structure, Phys Rev Lett 115, 193603 (2015).
- [18] T. T. Luu and H. J. Wörner, Measurement of the Berry curvature of solids using high-harmonic spectroscopy, Nat Commun 9, 916 (2018).
- [19] H. K. Avetissian and G. F. Mkrtchian, High laser harmonics induced by the Berry curvature in time-reversal invariant materials, Phys Rev B 102, 245422 (2020).
- [20] H. K. Avetissian, V. N. Avetisyan, B. R. Avchyan, and G. F. Mkrtchian, High-order harmonic generation in three-dimensional Weyl semimetals with broken timereversal symmetry, Phys Rev A 106, 033107 (2022).
- [21] T. T. Luu, Z. Yin, A. Jain, T. Gaumnitz, Y. Pertot, J. Ma, and H. J. Wörner, Extreme–ultraviolet high– harmonic generation in liquids, Nat Commun 9, 3723 (2018).
- [22] Y. S. You, Y. Yin, Y. Wu, A. Chew, X. Ren, F. Zhuang, S. Gholam-Mirzaei, M. Chini, Z. Chang, and S. Ghimire, High-harmonic generation in amorphous solids, Nat Commun 8, 724 (2017).
- [23] A.-W. Zeng and X.-B. Bian, Impact of statistical fluctuations on high harmonic generation in liquids, Phys Rev Lett 124, 203901 (2020).
- [24] C.-L. Xia, Z.-L. Li, J.-Q. Liu, A.-W. Zeng, L.-J. Lü, and X.-B. Bian, Role of charge-resonance states in liquid high-order harmonic generation, Phys Rev A 105, 013115 (2022).
- [25] Z.-W. Ding, Y.-B. Wang, Z.-L. Li, and X.-B. Bian, High-order harmonic generation in liquids in bicircularly polarized laser fields, Phys Rev A 107, 013503 (2023).
- [26] T. Huang, X. Zhu, L. Li, X. Liu, P. Lan, and P. Lu, High-order-harmonic generation of a doped semiconductor, Phys Rev A 96, 043425 (2017).
- [27] S. Almalki, A. M. Parks, G. Bart, P. B. Corkum, T. Brabec, and C. R. McDonald, High harmonic generation tomography of impurities in solids: conceptual analysis, Phys Rev B 98, 144307 (2018).
- [28] C. Yu, K. K. Hansen, and L. B. Madsen, High-order harmonic generation in imperfect crystals, Phys Rev A 99, 063408 (2019).
- [29] C. Yu, K. K. Hansen, and L. B. Madsen, Enhanced highorder harmonic generation in donor-doped band-gap materials, Phys Rev A 99, 013435 (2019).
- [30] C.-L. Xia, J.-Q. Liu, L.-J. Lü, A.-W. Zeng, Z.-L. Li, and X.-B. Bian, Theoretical study of high-order harmonic generation in solutions, J Phys B: At Mol Opt Phys 55,

- 045401 (2022).
- [31] G. Orlando, C.-M. Wang, T.-S. Ho, and S.-I. Chu, Highorder harmonic generation in disordered semiconductors, JOSA B 35, 680 (2018).
- [32] G. Orlando, T.-S. Ho, and S.-I. Chu, Macroscopic effects on high-order harmonic generation in disordered semiconductors, JOSA B 36, 1873 (2019).
- [33] K. Chinzei and T. N. Ikeda, Disorder effects on the origin of high-order harmonic generation in solids, Phys Rev Res 2, 013033 (2020).
- [34] P. W. Anderson, Absence of diffusion in certain random lattices, Phys Rev 109, 1492 (1958).
- [35] E. Abrahams, P. W. Anderson, D. C. Licciardello, and T. V. Ramakrishnan, Scaling theory of localization: Absence of quantum diffusion in two dimensions, Phys Rev Lett 42, 673 (1979).
- [36] F. Evers and A. D. Mirlin, Anderson transitions, Rev Mod Phys 80, 1355 (2008).
- [37] M. Lewenstein, P. Balcou, M. Y. Ivanov, A. L'huillier, and P. B. Corkum, Theory of high-harmonic generation by low-frequency laser fields, Phys Rev A 49, 2117 (1994).
- [38] A. Pattanayak, Á. Jiménez-Galán, M. Ivanov, and G. Dixit, High harmonic spectroscopy of disorderinduced Anderson localization, arXiv preprint arXiv:2101.08536 10.48550/arXiv.2101.08536 (2021).
- [39] H. W. Kroto, J. R. Heath, S. C. O'Brien, R. F. Curl, and R. E. Smalley, C60: Buckminsterfullerene, Nature 318, 162 (1985).
- [40] S. Iijima, Helical microtubules of graphitic carbon, Nature 354, 56 (1991).
- [41] A. D. Güçlü, P. Potasz, M. Korkusinski, and P. Hawrylak, *Graphene quantum dots* (Springer, 2014).
- [42] P. W. Fowler and D. E. Manolopoulos, An atlas of fullerenes (Courier Corporation, 2007).
- [43] G. P. Zhang, Optical high harmonic generation in C 60, Phys Rev Lett 95, 047401 (2005).
- [44] G. P. Zhang and T. F. George, Ellipticity dependence of optical harmonic generation in C 60, Phys Rev A 74, 023811 (2006).
- [45] G. P. Zhang and Y. H. Bai, High-order harmonic generation in solid C 60, Phys Rev B 101, 081412 (2020).
- [46] H. K. Avetissian, A. G. Ghazaryan, and G. F. Mkrtchian, High harmonic generation in fullerene molecules, Phys Rev B 104, 125436 (2021).
- [47] A. Pattanayak, M. S. Mrudul, and G. Dixit, Influence of vacancy defects in solid high-order harmonic generation, Phys Rev A 101, 013404 (2020).
- [48] H. Iravani, K. K. Hansen, and L. B. Madsen, Effects of vacancies on high-order harmonic generation in a linear chain with band gap, Phys Rev Res 2, 013204 (2020).
- [49] T. Hansen and L. B. Madsen, Doping effects in highharmonic generation from correlated systems, Phys Rev B 106, 235142 (2022).
- [50] G. Orlando, M.-I. Lee, and T.-S. Ho, Ellipticity dependence of high-order harmonic generation in disordered semiconductors, J Phys B: At Mol Opt Phys 55, 185601 (2022).
- [51] K. Harigaya and S. Abe, Optical-absorption spectra in fullerenes C 60 and C 70: Effects of Coulomb interactions, lattice fluctuations, and anisotropy, Phys Rev B 49, 16746 (1994).

- [52] G. Chiappe, E. Louis, E. San-Fabián, and J. A. Vergés, Can model Hamiltonians describe the electron–electron interaction in π -conjugated systems?: PAH and graphene, J Condens Matter Phys **27**, 463001 (2015).
- [53] P. Schwerdtfeger, L. Wirz, and J. Avery, Program fullerene: a software package for constructing and analyzing structures of regular fullerenes, J Comput Chem 34, 1508 (2013).
- [54] J. E. Fischer and P. A. Heiney, Order and disorder in fullerene and fulleride solids, J Phys Chem Solids 54, 1725 (1993).
- [55] N. R. Tummala, Z. Zheng, S. G. Aziz, V. Coropceanu, and J.-L. Brédas, Static and dynamic energetic disorders in the C60, PC61BM, C70, and PC71BM fullerenes, J Phys Chem Lett 6, 3657 (2015).
- [56] G. d'Avino, Y. Olivier, L. Muccioli, and D. Beljonne, Do charges delocalize over multiple molecules in fullerene derivatives?, J Mater Chem C 4, 3747 (2016).

- [57] R. L. Martin and J. P. Ritchie, Coulomb and exchange interactions in C 60 n-, Phys Rev B 48, 4845 (1993).
- [58] Y. B. Lev and D. R. Reichman, Dynamics of many-body localization, Phys Rev B 89, 220201 (2014).
- [59] L. Kadanoff and G. Baym, Quantum Statistical Mechanics WA benjamin Inc, New York (1962).
- [60] L. V. Keldysh, Diagram technique for nonequilibrium processes, Sov Phys JETP 20, 1018 (1965).
- [61] B. Kramer and A. MacKinnon, Localization: theory and experiment, Rep Prog Phys 56, 1469 (1993).
- [62] G. P. Zhang, M. S. Si, M. Murakami, Y. H. Bai, and T. F. George, Generating high-order optical and spin harmonics from ferromagnetic monolayers, Nat Commun 9, 3031 (2018).
- [63] G. P. Zhang, Hartree-Fock Dynamical Electron-Correlation Effects in C 60 after Laser Excitation, Phys Rev Lett 91, 176801 (2003).
- [64] G. Vampa, C. McDonald, G. Orlando, P. Corkum, and T. Brabec, Semiclassical analysis of high harmonic generation in bulk crystals, Phys Rev B 91, 064302 (2015).